Calcified Tissue International (2024) 114:119–128
https://doi.org/10.1007/s00223-023-01153-5

ORIGINAL RESEARCH

Microarchitecture Alternations of Osteochondral Junction in Patients with Osteonecrosis of the Femoral Head

Pengbo Wang[1] · Xu Wang[1] · Hang Qian[1] · Jun Liu[1] · Gang Liu[2] · Ruisong Wang[3] · Ruiyu Liu[1]

Received: 7 May 2023 / Accepted: 6 October 2023 / Published online: 30 November 2023

Abstract

The study was aimed to investigate microarchitecture of osteochondral junction in patients with osteonecrosis of the femoral head (ONFH). We hypothesis that there were microarchitecture alternations in osteochondral junction and regional differences between the necrotic region (NR) and adjacent non-necrotic region(ANR) in patients with ONFH. Femoral heads with ONFH or femoral neck fracture were included in ONFH group ($n=11$) and control group ($n=11$). Cylindrical specimens were drilled on the NR/ANR of femoral heads in ONFH group and matched positions in control group (CO.NR/ CO.ANR). Histology, micro-CT, and scanning electron microscope were used to investigate microarchitecture of osteochondral junction. Layered analysis of subchondral bone plate was underwent. Mankin scores on NR were higher than that on ANR or CO.NR, respectively ($P<0.001$, $P<0.001$). Calcified cartilage zone on the NR and ANR was thinner than that on the CO.NR and CO.ANR, respectively ($P=0.002$, $P=0.002$). Tidemark roughness on the NR was larger than that on the ANR ($P=0.002$). Subchondral bone plate of NR and ANR was thicker than that on the CON.NR and CON.ANR, respectively ($P=0.002$, $P=0.009$). Bone volume fraction of subchondral bone plate on the NR was significantly decreasing compared to ANR and CON.NR, respectively ($P=0.015$, $P=0.002$). Subchondral bone plate on the NR had larger area percentages and more numbers of micropores than ANR and CON.NR ($P=0.002/0.002$, $P=0.002/0.002$). Layered analysis showed that bone mass loss and hypomineralization were mainly on the cartilage side of subchondral bone plate in ONFH. There were microarchitecture alternations of osteochondral junction in ONFH, including thinned calcified cartilage zone, thickened subchondral bone plate, decreased bone mass, altered micropores, and hypomineralization of subchondral bone plate. Regional differences in microarchitecture of osteochondral junction were found between necrotic regions and adjacent non-necrotic regions. Subchondral bone plate in ONFH had uneven distribution of bone volume fraction and bone mineral density, which might aggravate cartilage degeneration by affecting the transmission of mechanical stresses.

Keywords Osteonecrosis of the femoral head · Osteochondral junction · Microarchitecture alternations · Regional differences · Hypomineralization

Introduction

Osteonecrosis of the femoral head (ONFH) is a debilitating disease primarily affecting patients in the 3rd–5th decades of life, which progresses to femoral head collapse and leads to total hip arthroplasty before the age of 50 [1–3]. Glucocorticoid use is the most common cause of ONFH and associated with > 50% of the cases [4]. Compared to primary osteoarthritis (OA) patients, patients with ONFH are younger, and hip preservation treatment is more appropriate especially before collapse of the femoral head. Preventing cartilage degeneration and collapse of the femoral head for patients with ONFH could be the key point for hip preservation therapy.

✉ Ruiyu Liu
liuryu@126.com

[1] Department of Orthopedics, The Second Affiliated Hospital of Xi'an Jiaotong University, Xi'an Jiaotong University, Xi'an 710049, China

[2] Department of Orthopedics, Xi'an Daxing Hospital, Xi'an 710000, China

[3] Department of Orthopedics, Xi'an Fifth Hospital, Xi'an 710000, China

Currently, hip preservation therapy for ONFH focuses more on bone reconstruction in necrotic regions. Alterations of subchondral trabeculae in necrotic region are suspected to have a predominant role on collapse of the femoral head [5]. However, core decompression combined with bone grafting has been only shown to have good results in early-stage patients, but not effective in moderate/advanced-stage patients [6]. Cartilage degeneration has not been inhibited, which was one of critical problems. Osteochondral junction is a transitional region between articular cartilage and subchondral bone and closely associated with cartilage function. It has been neglected in hip preservation therapy, and few studies have focused on this region of ONFH, especially its microarchitecture.

Osteochondral junction is composed of mineralized calcified cartilage zone (CCZ) and subchondral bone plate(SCP). It plays multiple roles between the subchondral bone and the cartilage [7] (Fig. 1). Previous studies have confirmed that it was associated with the aggravation of OA [8, 9]. In OA, bottom-up calcification thickens the calcified cartilage region, which disrupts the cartilage structure, and the sclerosis of SCP in response to the mechanical stress leads to cartilage degeneration [10, 11]. Therefore, studying osteochondral junction of ONFH will beneficial to understand its impact on cartilage degeneration and femoral head collapse, and provide new insights into hip preservation therapies.

The study was aimed to investigate microarchitecture of osteochondral junction in ONFH by histology, micro-CT, and scanning electron microscope (SEM). We hypothesis that there are microarchitecture alternations in osteochondral junction and regional differences between the necrotic region and adjacent non-necrotic region in patients with ONFH.

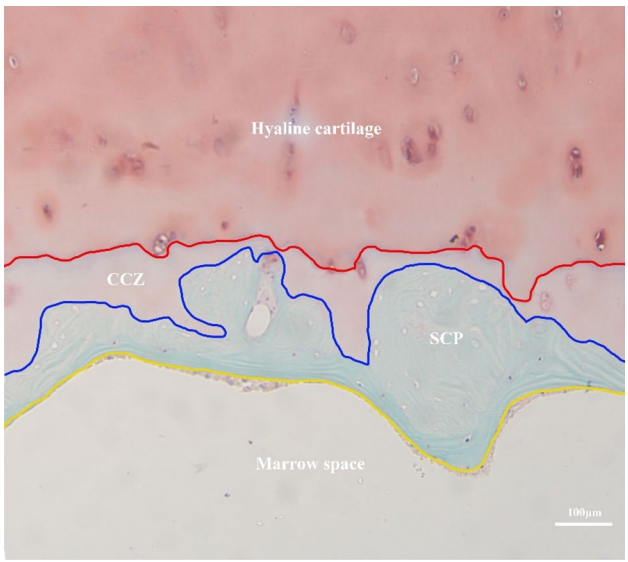

Fig. 1 The osteochondral junction composed of calcified cartilage zone and subchondral bone plate is between the red and yellow lines (Color figure online)

Methods

Study Population

Patients were recruited from the Second Affiliated Hospital of Xi'an Jiaotong University in China from January 2022 to April 2023. Patients were enrolled in ONFH group (ONFH) and control group (Control) based on their diagnosis. Inclusion criteria: (1) Patients were diagnosed with ONFH-staged ARCO III [12] or femoral neck fracture due to acute trauma before operations. (2) Patients with ONFH had a history of glucocorticoid use. (3) Patients underwent total hip arthroplasty. Exclusion criteria: (1) Patients with ONFH had a history of alcohol abuse, hip trauma, or diving. (2) Patients had osteoporosis, diabetes mellitus, malignant diseases, any signs of hip OA or other joint diseases. (3) It was no more than 2 days from injury to operations for patients with femoral neck fracture. Clinical data [age, sex, and body mass index (BMI)] were collected. The study was in accordance with The Code of Ethics of the World Medical Association. Patients signed informed consent before this study. The study had been approved by the Human Ethics Committees of Xi'an Jiaotong University (2022–776).

Processing of Tissue

Femoral heads were washed by normal saline to remove residual blood. All necrosis regions of ONFH were located on the anterosuperior aspect of femoral heads (Fig. 2a). To avoid individual difference of femoral heads, radius of the femoral head was defined and measured: the smallest external circle was drew based on horizontal view of the femoral head, and the radius of circle was defined as radius of the femoral head, L_1 (Fig. 2b). Cylindrical specimens with diameter of 5 mm and length of (6–8) mm were drilled on the necrotic region (NR) and adjacent non-necrotic region (ANR) of ONFH femoral heads (Fig. 2c). As for Control, specimens were drilled on the anterosuperior aspect (CO.NR) and lateral aspect (CO.ANR), which were corresponded to NR and ANR in ONFH. All specimens were embalmed in a 10% neutral buffered formalin solution or a 2.5% glutaraldehyde solution, and were stored in sealed containers at 4 °C.

Micro-CT

Specimens were washed repeatedly with phosphate buffer saline to remove potential bone debris and scanned by a high-definition micro-CT (SkyScan1276, Bruker). The following settings were used for projection image acquisition: X-ray tube voltage = 50 kV, X-ray tube current = 200 mA, exposure time = 1500 ms, filter = 0.5 mm Al, frame

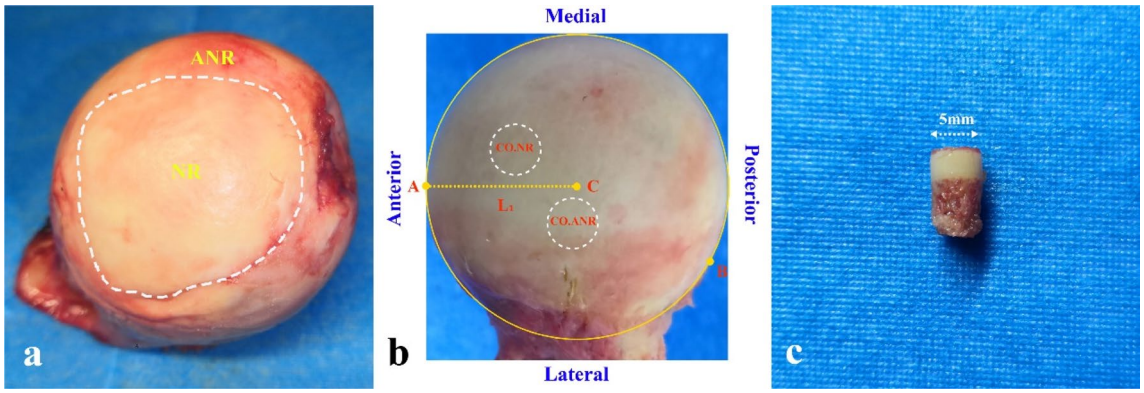

Fig. 2 **a**: Femoral heads diagnosed as ONFH were divided into NR (white circle) and ANR; **b**: Horizontal view of the femoral head: CO.NR and CO.ANR were sites drilled in Control; A and B were the 2 points of the smallest external circle of the femoral head. C and L1 were the center and radius of the circle, respectively; **c**: Cylindrical specimens were drilled on the femoral heads. NR was the necrotic region in ONFH; ANR was the adjacent non-necrotic region in ONFH; CO.NR was the site corresponding to NR of ONFH and located on the anterosuperior aspect in Control; CO.ANR was the site corresponding to ANR of ONFH and located on the lateral aspect in Control (Color figure online)

averaging = 3, amount of projection images = 1200, and isotropic voxel size = 2.8 mm. Projections were reconstructed with Nrecon software (v1.6.9.8) with beam hardening and ring artifact corrections applied. The outer 100-μm rim of the specimens was excluded to avoid incorporating potential bone debris and other artifacts.

The volume of interests (VOI), located at SCP, was a cylinder with a diameter of 2000 μm and a height as the same as the thickness of SCP. It had typical porous structure, and the pore wall was similar to trabecular bone [11]. Thus, bone volume fraction (BVF), bone mineral density (BMD), trabecular thickness, trabecular number, trabecular separation, and open porosity percentage of the VOI were measured and analyzed. Furthermore, the VOI was divided equally into 5 equal parts based on the thickness of SCP. These parts were defined as zones 1, 2, 3, 4, and 5 along the cartilage to marrow space (Fig. 3a). BMD and BVF of 5 zones were measured and analyzed. On 3D reconstructed images of specimens, cartilage was segmented to expose SCP surface (Fig. 3b, c). Area percentages and numbers of micropores were measured and analyzed by Fiji software.

Histology

Specimens were decalcified for 8 weeks using EDTA after micro-CT scanning. They were dehydrated using ascending concentrations of ethanol (70–100%), embedded in paraffin wax, and sectioned coronally (5 μm). Sections were stained by Safranin O/Fast Green, hematoxylin–eosin, Masson, and Sirius red. Finally, sections were dehydrated through serial dilutions of ethanol, cleared in xylene, and mounted using neutral gum. A light microscopy was used to observe Safranin O/Fast Green,

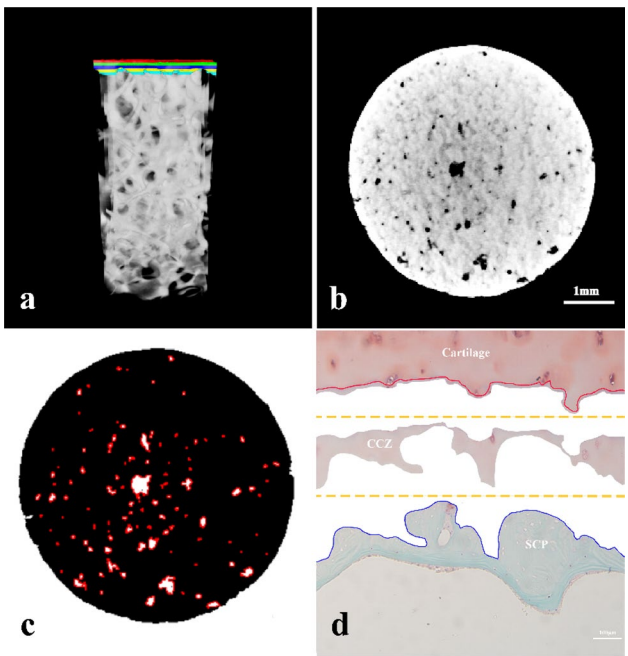

Fig. 3 **a**: SCP was divided equally into 5 equal parts, which were displayed in 5 colors; **b** and **c** were SCP surface images scanned by micro-CT, which showed micropores; **d**: Images stained by Safranin O/Fast Green showed microarchitectures of osteochondral junction(100×). The red line, blue line, and yellow-dotted line were tidemark, cement line, and projected length of CCZ, respectively (Color figure online)

hematoxylin–eosin or Masson staining sections. Polarized light microscope was used to observe Sirius red staining sections. The following parameters were measured and analyzed by Fiji software (Fig. 3d):

- Mankin score: Articular cartilage of Safranin O/Fast Green sections was assessed by 2 experienced pathologists using Mankin's grading system by double-blind principle[13].
- Mean thickness of CCZ: Area of CCZ divided by the projected length of CCZ on Safranin O/Fast Green sections[14].
- Mean thickness of SCP: Area of SCP divided by the projected length of CCZ on Safranin O/Fast Green sections.
- Roughness of tidemark and cement line: The true length of the tidemark and the cement line divided by the projected length of CCZ on Safranin O/Fast Green sections [15]. The two parameters could reflect microarchitecture alterations between hyaline cartilage and calcified cartilage, calcified cartilage, and subchondral bone plate, respectively.
- Bone maturity degrees: Red areas percentage to SCP on Masson staining sections.
- Collagen fibers alignment: Orientation frequency of collagen fibers in SCP was measured by OrientationJ(a plugin of Fiji) on Sirius red staining sections.

Scanning Electron Microscope

Specimens were fixed in 2.5% glutaraldehyde at 4 °C for 24 h. After gradient alcohol dehydration and hexamethyldisilane-replacing alcohol, specimens were frozen in liquid nitrogen for 3 h and divided into two parts along cartilage-marrow axis. Natural sections of specimens were observed by SEM (Gemini SEM 500, Carl Zeiss) after metal spraying. Ultrastructure of osteochondral junction, such as interlocking, imbedding, and so on, were observed [16].

Statistics Analysis

Statistical analyses were performed by SPSS version 22. Quantitative variables were expressed as mean ± standard deviation ($\bar{x}\pm s$). Qualitative variables were expressed as numbers (%). Mann–Whitney U test was used for comparisons between 2 groups. χ^2 test was used for comparisons between groups. Significance level was set at 5%.

Results

Patients

A total of 22 femoral heads were enrolled in ONFH ($n=11$) and Control ($n=11$). The age of ONFH (43.73 ± 13.78 years) was lower than that of Control (63.73 ± 3.19) ($P<0.001$). There was no significant difference in BMI and sex between ONFH [(23.95 ± 1.74) kg/m^2, 7/4(man/female)], and Control[(23.20 ± 1.71) kg/m^2, 5/6(man/female)]($P=0.225$, 0.392).

Cartilage Degeneration

Safranin O/Fast Green sections showed that cartilage on the NR of ONFH had severe staining deficits, disorganized chondrocytes arranged in clusters, and broken tidemark, which illustrated pronounced cartilage degeneration. Semi-quantitative analysis based on the Mankin score indicated that scores on NR (4.55 ± 1.63) were higher than that on ANR (0.91 ± 0.70) or CO.NR (0.65 ± 0.61), respectively ($P<0.001$, $P<0.001$)(Fig. 4). These results suggested that there was significant degeneration of cartilage in patients with ONFH and regional differences in the degree of cartilage degeneration on NR and ANR.

CCZ, Tidemark, and Cement Line

The osteochondral junction on the NR of ONFH showed significantly more tidemark duplication, interruption, and few chondrocytes on hematoxylin–eosin sections (Fig. 5). In order to eliminate individual differences, CCZ thickness

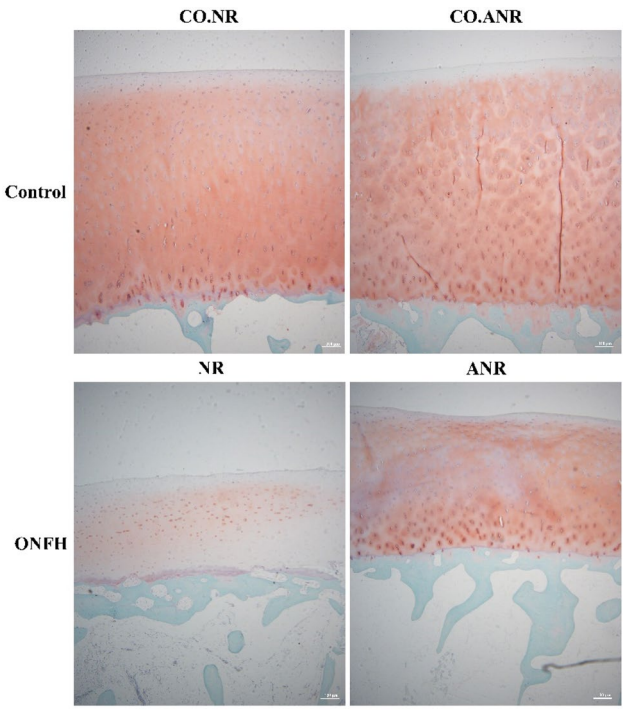

Fig. 4 Cartilage degeneration among different regions in ONFH and Control (Safranin O/Fast Green staining,×40). NR was the necrotic region in ONFH; ANR was the adjacent non-necrotic region in ONFH; CO.NR was the site corresponding to NR of ONFH and located on the anterosuperior aspect in Control; CO.ANR was the site corresponding to ANR of ONFH and located on the lateral aspect in Control

was adjusted by the femoral head radius (L_1). CCZ on the NR was thinner than that on the ANR ($P=0.026$). CCZ on the NR and ANR were thinner than that on the CO.NR and CO.ANR, respectively ($P=0.002$, $P=0.002$). Tidemark roughness on the NR was larger than that on the ANR and CO.NR ($P=0.002$, $P=0.002$). Cement line roughness on the NR and ANR was smaller than on the CO.NR and CO.ANR, respectively ($P=0.002$, $P=0.002$) (Table1).

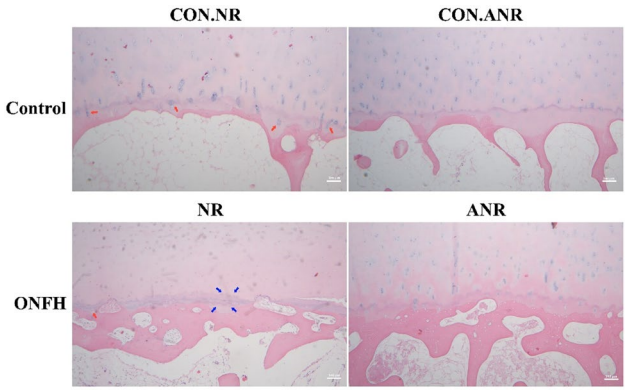

Fig. 5 CCZ, tidemark, and cement line among different regions in ONFH and Control (Hematoxylin–eosin staining, ×40). A red arrow indicated chondrocytes in the CCZ. A blue arrow indicated widened tidemark on the NR. NR was the necrotic region in ONFH; ANR was the adjacent non-necrotic region in ONFH; CO.NR was the site corresponding to NR of ONFH and located on the anterosuperior aspect in Control; CO.ANR was the site corresponding to ANR of ONFH and located on the lateral aspect in Control (Color figure online)

Microarchitecture of SCP

SCP was the important transition region between articular cartilage and subchondral bone, and its microarchitecture alternations were strongly associated with cartilage degeneration and femoral head collapse. The adjustment method of SCP thickness was same as that of CCZ. SCP on the NR and ANR was thicker than that on the CON.NR and CON.ANR, respectively ($P=0.002$, $P=0.009$). Meanwhile, SCP on the NR was thicker than that on the ANR ($P=0.040$). SCP on the NR had larger area percentages and more numbers of micropores than ANR and CON.NR ($P=0.002/0.002$, $P=0.002/0.002$). Bone mass showed regional differences: BVF on the NR was significantly decreasing compared to ANR and CON.NR, respectively ($P=0.015$, $P=0.002$). Interestingly, regional differences between NR and CO.NR were not showed on BMD ($P=0.180$). As for intrinsic microstructure of SCP, trabecular thickness, trabecular separation, and open porosity of SCP showed regional differences between NR and CO.NR except for trabecular number($P=0.002$, $P=0.004$, $P=0.004$, $P=0.065$). The results showed microstructure alternations in SCP of ONFH, including thickness, micropores, bone mass, and so on. Moreover, there were significant regional differences in microstructure between NR and ANR (Table.1).

Collagen Fibers and Hypomineralization of SCP

Mature collagen fibers of bone were stained red on the Masson staining sections, and collagen fibers alignment could be identified by Sirius red staining. Maturity degree and

Table 1 Comparison of parameters among different regions in ONFH and control

Parameters	ONFH		Control	
	NR	ANR	CO.NR	CO.ANR
Adjusted CCZ thickness (%)	0.35 ± 0.03^{ab}	0.30 ± 0.03^{c}	0.44 ± 0.03	0.47 ± 0.02
Roughness of tidemark	1.32 ± 0.05^{ab}	1.16 ± 0.05	1.17 ± 0.02	1.17 ± 0.03
Roughness of cement line	1.24 ± 0.11^{b}	1.33 ± 0.16^{c}	1.67 ± 0.12	1.67 ± 0.05
Adjusted SCP thickness(%)	1.73 ± 0.25^{ab}	1.46 ± 0.25^{c}	1.07 ± 0.08	0.90 ± 0.07
Area percentages of micropores (%)	13.47 ± 1.29^{ab}	9.02 ± 1.31	7.85 ± 0.48	7.29 ± 0.86
Numbers of micropores ($1/\mu m^2$)	20.25 ± 2.37^{ab}	12.52 ± 2.70^{c}	8.40 ± 1.78^{c}	4.25 ± 1.10
BVF (%)	23.78 ± 3.14^{ab}	28.34 ± 1.00^{c}	40.92 ± 7.87	41.58 ± 8.12
BMD (mg/cm^3)	203.53 ± 67.89	216.52 ± 31.84	280.04 ± 104.40	256.18 ± 86.64
Trabecular thickness of SCP(mm)	0.21 ± 0.01^{b}	0.21 ± 0.03^{c}	0.29 ± 0.05	0.26 ± 0.04
Trabecular number of SCP(1/mm)	1.00 ± 0.24	1.35 ± 0.22	1.35 ± 0.22	1.35 ± 0.24
Trabecular separation of SCP(mm)	0.40 ± 0.03^{b}	0.35 ± 0.04	0.33 ± 0.04	0.32 ± 0.03
Open porosity (%)	77.86 ± 5.48^{ab}	64.64 ± 4.92	62.39 ± 8.64	63.40 ± 6.12
Red areas (%)	12.76 ± 0.81^{ab}	7.53 ± 2.37^{c}	26.26 ± 1.53	23.67 ± 1.87

Compared to ANR, $^{a}P<0.05$; Compared to CO.NR, $^{b}P<0.05$; Compared to CO.ANR, $^{c}P<0.05$; NR was the necrotic region in ONFH; ANR was the adjacent non-necrotic region in ONFH; CO.NR was the site corresponding to NR of ONFH and located on the anterosuperior aspect in Control; CO.ANR was the site corresponding to ANR of ONFH and located on the lateral aspect in Control

collagen fibers alignment of SCP were evaluated in various regions (Fig. 6). NR had more red areas than ANR ($P=0.002$), while less red areas than CO.NR ($P=0.002$) (Table.1). Birefringent collagen fibers in ONFH showed qualitatively less alignment compared to Control. Upon quantification, collagen linearity was significantly smaller in ONFH ($P<0.001$)(Fig. 7). Furthermore, SEM showed that the ultrastructure between CCZ and SCP was intact in both groups, while hypomineralization was pronounced in ONFH (Fig. 8).

Layered Microarchitecture of SCP

Previous results showed that the BVF of SCP had regional differences. To investigate microarchitecture furtherly, layered microarchitecture analysis was underwent. SCP in both groups had uneven distribution of BMD and BVF, which displayed a trend of high in the middle and low on both sides. BMD of NR-5 was larger than that of CO.NR-5 ($P=0.002$), but BMD of NR-1 was smaller ($P=0.009$). Moreover, BVF of NR-1, NR-2, and NR-3 were significantly smaller than CO.NR-1, CO.NR-2, and CO.NR-3, respectively ($P=0.015$, $P=0.004$, $P=0.026$). Uneven distribution of BMD and BVF indicated that bone mass loss and hypomineralization were mainly on the cartilage side of SCP. Notably, the difference in BMD between NR-5 and CO.NR-5 suggested that there was more bone formation on the marrow space side of SCP in ONFH (Fig. 9), which was consistent with the result of Masson staining.

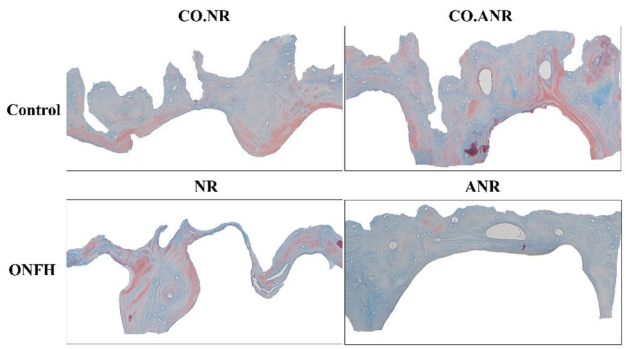

Fig. 6 Comparison of SCP maturity among different regions in ONFH and Control. NR was the necrotic region in ONFH; ANR was the adjacent non-necrotic region in ONFH; CO.NR was the site corresponding to NR of ONFH and located on the anterosuperior aspect in Control; CO.ANR was the site corresponding to ANR of ONFH and located on the lateral aspect in Control

Discussion

To date, there has been no consensus on the pathophysiological mechanisms of ONFH. Most studies focused on the necrotic areas and ignored the pathological changes in the osteochondral junction of ONFH. In this study, we focused on the osteochondral junction of ONFH, and demonstrated microarchitecture alternations by comparison with healthy femoral heads, including thinned CCZ, thickened SCP, decreased bone mass and altered micropores. Meanwhile, there were significant regional differences in microarchitecture between the necrotic region and adjacent non-necrotic region, which were consistent with the regional difference of cartilage degeneration degree. Layered analysis of SCP demonstrated bone mass loss and hypomineralization distributed on the cartilage side of SCP, and it provided new insights for studying on pathological mechanism of ONFH.

CCZ is the transitional structure between hyaline cartilage and the subchondral bone, which plays a role in stabilizing articular cartilage, connection, biomechanics transfer, and crosstalk between bone and cartilage [7]. Rasmus et al. found that thickness of CCZ was increasing with progress of primary OA, which was attributed to endochondral ossification [8]. In later study, they found decreased thickness of CCZ in rheumatoid arthritis because of inflammation [9]. These results indicated changes of CCZ affected upper cartilage by different pathological mechanisms. In the present study, decreased thickness of CCZ was found, which was similar to rheumatoid arthritis. Compared to OA and rheumatoid arthritis, cartilage degeneration in ONFH was mostly located on the necrotic region. Thinned CCZ made the distance shorter between hyaline cartilage and subchondral bone. Therefore, CCZ might been affected by inflammation factors from the necrotic region, and cartilage degeneration was driven. Several studies have found tidemark and cement

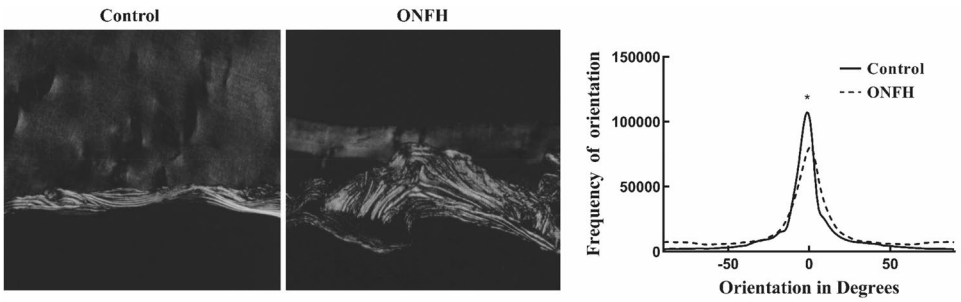

Fig. 7 Comparison of SCP collagen fibers alignment between ONFH and Control. * was defined as $P<0.05$

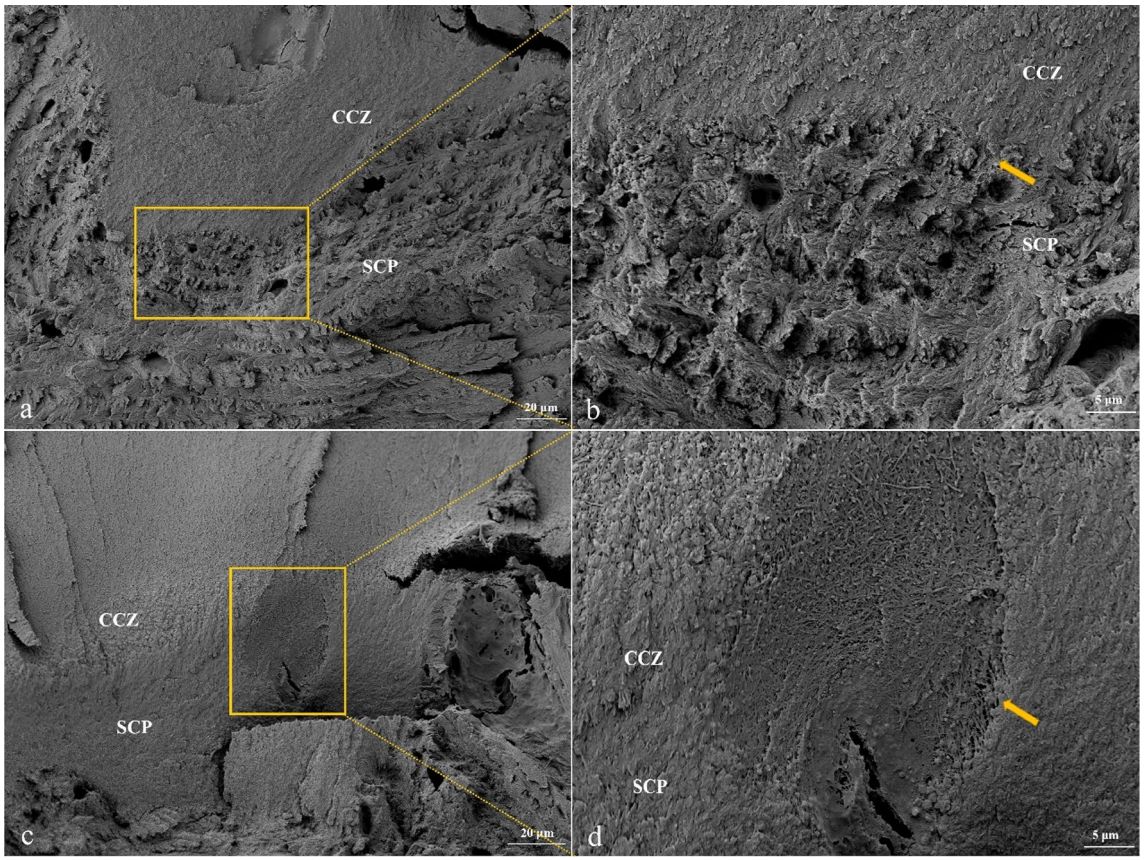

Fig. 8 The ultrastructure between CCZ and SCP observed by SEM. **a**: imbedding structure between CCZ and SCP in Control(×500); **b**: yellow box in a. Yellow arrow showed the ultrastructure between CCZ and SCP was intact (×2000); **c**: interlocking structure between CCZ and SCP in ONFH (×500); **d**: yellow box in c. Yellow arrow showed pronounced hypomineralization (×2000) (Color figure online)

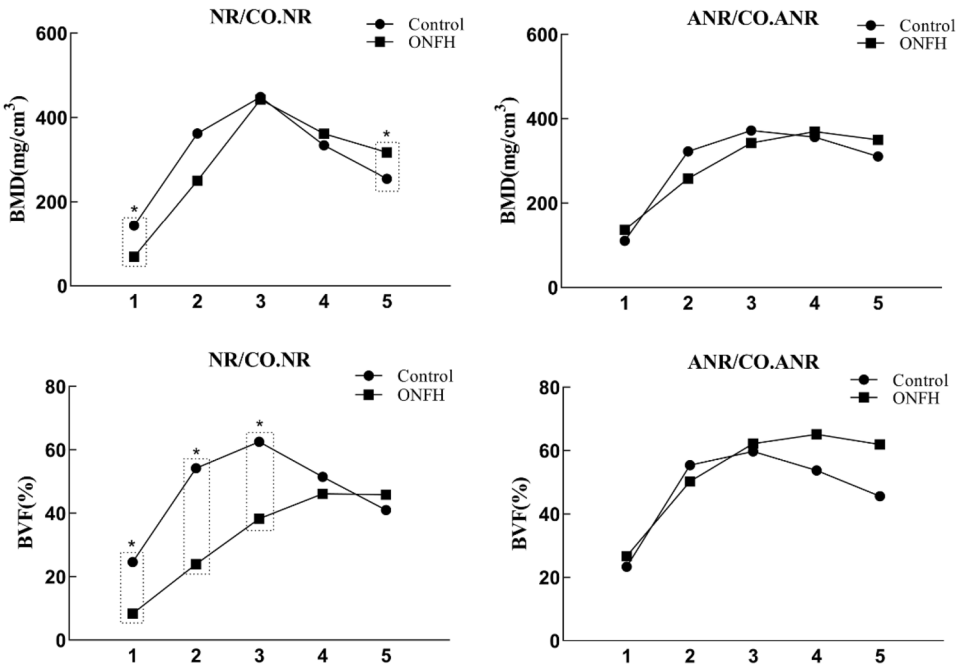

Fig. 9 Comparison of BMD and BVF for layered microarchitecture among different regions in ONFH and Control. * was defined as $P < 0.05$; NR was the necrotic region in ONFH; ANR was the adjacent non-necrotic region in ONFH; CO.NR was the site corresponding to NR of ONFH and located on the anterosuperior aspect in Control; CO.ANR was the site corresponding to ANR of ONFH and located on the lateral aspect in Control

line was highly correlated with cartilage degeneration [15, 17]. The present study showed that regional differences in roughness of tidemark and cement line were consistent with distribution of cartilage degeneration degree, which demonstrated the effect of the necrotic region on the cartilage again.

Cortical and cancellous bone maintains healthy structure by balanced bone turnover [18]. A previous study found that SCP of ONFH exhibited no changes in composition nor structure compared to femoral heads with OA, while there was lower volume fraction of subchondral trabecular bone [5]. These changes could be attributed to increased but unbalanced bone turnover. However, SCP of femoral heads was thickened in patients with advanced-stage OA compared to healthy people [9]. Therefore, we included healthy femoral heads in the control group to investigate the microstructure of SCP in ONFH. Compared to healthy femoral heads, SCP of ONFH was thickened but had a lower bone volume fraction. Likewise, regional differences were exhibited in thickness and bone volume fraction of SCP in ONFH. Less alignment of collagen fibers indicated the dysfunction of bone remodeling, which might be affected by the necrotic region. The biomechanical properties would also change as a result of microstructure alternations, which could be accounted for severer cartilage degeneration on the necrotic region.

SCP is the typical porous structure and numerous micropores connect the cartilage to subchondral bone. Imhof et.al have demonstrated that micropores of SCP were pathways for a nutrition of chondrocytes lying close to tidemark [19]. In the present study, we analyzed porous characters of SCP by micro-CT. Decreased thickness and increased separation of pore walls indicated larger space of SCP but weaker support in ONFH. The porous alternations of SCP, combined with regional differences in bone volume fraction between the necrotic region and adjacent non-necrotic region, might be accounted for the collapse of femoral heads with ONFH. Meanwhile, it might be one of the reasons for the collapse that a step structure because of differences in thickness of SCP would accumulate stress concentration [20]. A previous study demonstrated that load-bearing region had larger area and more numbers of micropores in healthy femoral heads [21]. The difference was consistent with cartilage thickness distribution, which implied a crosstalk of micropores between cartilage and subchondral bone. In this study, more area and numbers of micropores in ONFH were found. The alternation of micropores and thinned CCZ allowed for more exchange of substances from necrotic regions to cartilage, which could illustrate cartilage degeneration was observed at early-stage in ONFH by Delayed Gadolinium-Enhanced Magnetic Resonance Imaging [22].

To investigate microarchitecture alterations furtherly, we divided SCP and made a layered analysis. There was more hypomineralization on the zone of SCP close to cartilage. SEM images between CCZ and SCP also supported above results. Several studies found chondrocytes transformed into hypertrophic chondrocytes with the stimulation of inflammatory factors from necrotic bone tissue and changes of microenvironment, which displayed more catabolism than synthesis [23, 24]. Catabolic molecules secreted by hypertrophic chondrocytes influenced peripheral cartilage matrix and bone matrix, such as matrix metallopeptidase 13, Indian hedgehog, and so on. On the other hand, apoptotic osteocytes of SCP close to cartilage-influenced osteoclast differentiation and bone remodeling by releasing factors that instructed neighboring viable osteocytes to produce receptor activator of nuclear factor κB ligand (RANKL) [25]. The unbalanced bone turnover because of increasing osteoclast might be another cause of hypomineralization. Uneven distribution of BMD and BVF in SCP affected the transmission of mechanical stresses and aggravated cartilage degeneration.

Our study found microstructure alternations of osteochondral junction in ONFH. The overlap of cartilage degeneration and microstructure alternations distributions indicated that osteochondral junction played a great role in the progress of ONFH. The necrotic region might affect upper cartilage by altering adjacent osteochondral junction. These results will be helpful to provide new insight for hip preservation therapy. Moreover, identified porous structure and layered analysis of SCP will give new ideas to design bioengineered materials for bone graft-treating ONFH.

Limitations of this study include as follows: (1) The sample size included in the study was not large because of finite ARCO stage III ONFH patients. (2) Age distribution of patients in 2 groups was different because of the limitation in sourcing healthy femoral heads. However, previous study demonstrated that the thickness and volume of the subchondral bone plate were not correlated with age [26]. In further study, we hope that sex and age-matching healthy femoral heads could be harvested and included in the control group. Moreover, the mechanism how the necrotic region affects osteochondral junction and cartilage will be the key point of our study.

Conclusion

This study showed microarchitecture alternations of osteochondral junction in ONFH, including thinned CCZ, thickened SCP, decreased bone mass, altered micropores, and hypomineralization of SCP. Regional differences in microarchitecture of osteochondral junction were found between necrotic regions and adjacent non-necrotic regions of ONFH. They were consistent with cartilage degeneration distribution, which demonstrated the necrotic region might

be the driven reason for cartilage degeneration and collapse of femoral heads with ONFH. Uneven distribution of BMD and BVF in SCP might aggravate cartilage degeneration by affecting the transmission of mechanical stresses. Hypomineralization of SCP distributing on the cartilage side provided a direction for studying the mechanism of necrotic regions affecting osteochondral junction.

Acknowledgements We acknowledge the Molecular Testing Center of Xi'an Jiaotong University where scanning electron microscope (SEM) images were taken.

Authors Contributions PW, XW, HQ, and RL participated to the conception and design of the study, acquisition of data, analysis, and interpretation of data, drafted the article, or revised it critically for important intellectual content and gave their final approval of the version to be submitted. JL, GL, and RW participated to the harvest of materials, the acquisition, and interpretation of data.

Funding This work was supported by the National Natural Science Foundation of China [81772411] and Shaanxi Provincial Key R&D Programme [S2023-YF-YBSF-0229].

Declarations

Conflicts of interest Pengbo Wang, Xu Wang, Hang Qian, Jun Liu, Gang Liu, Ruisong Wang, and Ruiyu Liu declare that they have no conflicts of interest.

Human and Animal Rights This study was approved by the ethical review Committee of the Second Affiliated Hospital of Xi'an Jiaotong University and was performed in accordance with the ethical standards as laid down in the 1964 Declaration of Helsinki and its later amendments.

Informed Consent All participants gave written-informed consent before entering the study.

References

1. Mont MA, Salem HS, Piuzzi NS, Goodman SB, Jones LC (2020) Nontraumatic osteonecrosis of the femoral head: where do we stand today? A 5-year update. J Bone Joint Surg Am 102:1084–1099. https://doi.org/10.2106/JBJS.19.01271
2. Choi HR, Steinberg ME, Cheng EY (2015) Osteonecrosis of the femoral head: diagnosis and classification systems. Curr Rev Musculoskelet Med 8:210–220. https://doi.org/10.1007/s12178-015-9278-7
3. Zalavras CG, Lieberman JR (2014) Osteonecrosis of the femoral head: evaluation and treatment. J Am Acad Orthop Surg 22:455–464. https://doi.org/10.5435/JAAOS-22-07-455
4. Kubo Y, Yamamoto T, Motomura G, Tsukamoto N, Karasuyama K, Sonoda K, Hatanaka H, Utsunomiya T, Iwamoto Y (2015) MRI-detected bone marrow changes within 3 weeks after initiation of high-dose corticosteroid therapy: a possible change preceding the subsequent appearance of low-intensity band in femoral head osteonecrosis. Rheumatol Int 35:1909–1912. https://doi.org/10.1007/s00296-015-3346-6
5. Pascart T, Falgayrac G, Cortet B, Paccou J, Bleuse M, Coursier R, Putman S, Quinchon JF, Bertheaume N, Delattre J, Marchandise P, Cultot A, Norberciak L, Kerckhofs G, Budzik JF (2022) Subchondral involvement in osteonecrosis of the femoral head: insight on local composition, microstructure and vascularization. Osteoarthritis Cartilage 30:1103–1115. https://doi.org/10.1016/j.joca.2022.05.003
6. D'Ambrosi R, Biancardi E, Massari G, Ragone V, Facchini RM (2018) Survival analysis after core decompression in association with platelet-rich plasma, mesenchymal stem cells, and synthetic bone graft in patients with osteonecrosis of the femoral head. Joints 6:16–22. https://doi.org/10.1055/s-0038-1626740
7. Wang F, Ying Z, Duan X, Tan H, Yang B, Guo L, Chen G, Dai G, Ma Z, Yang L (2009) Histomorphometric analysis of adult articular calcified cartilage zone. J Struct Biol 168:359–365. https://doi.org/10.1016/j.jsb.2009.08.010
8. Klose-Jensen R, Hartlev LB, Thomsen JS, Nyengaard JR, Boel LWT, Laursen M, Laurberg TB, Stengaard-Pedersen K, Hauge EM (2021) Calcified cartilage in patients with osteoarthritis of the hip compared to that of healthy subjects. A design-based histological study Bone 143:115660. https://doi.org/10.1016/j.bone.2020.115660
9. Jensen R, Christensen AF, Hartlev LB, Thomsen JS, Boel L, Laursen M, Revald PH, Varnum C, Keller KK, Hauge EM (2022) Calcified cartilage differs in patients with end-stage primary osteoarthritis and secondary osteoarthritis due to rheumatoid arthritis of the hip joint. Scand J Rheumatol 51:441–451. https://doi.org/10.1080/03009742.2021.1952754
10. Wang X, Wu Q, Zhang R, Fan Z, Li W, Mao R, Du Z, Yao X, Ma Y, Yan Y, Sun W, Wu H, Wei W, Hu Y, Hong Y, Hu H, Koh YW, Duan W, Chen X, Ouyang H (2023) Stage-specific and location-specific cartilage calcification in osteoarthritis development. Ann Rheum Dis 82:393–402. https://doi.org/10.1136/ard-2022-222944
11. Goldring SR (2012) Alterations in periarticular bone and cross talk between subchondral bone and articular cartilage in osteoarthritis. Ther Adv Musculoskelet Dis 4:249–258. https://doi.org/10.1177/1759720X12437353
12. Sultan AA, Mohamed N, Samuel LT, Chughtai M, Sodhi N, Krebs VE, Stearns KL, Molloy RM, Mont MA (2019) Classification systems of hip osteonecrosis: an updated review. Int Orthop 43:1089–1095. https://doi.org/10.1007/s00264-018-4018-4
13. Salo PT, Hogervorst T, Seerattan RA, Rucker D, Bray RC (2002) Selective joint denervation promotes knee osteoarthritis in the aging rat. J Orthop Res 20:1256–1264. https://doi.org/10.1016/S0736-0266(02)00045-1
14. Hofstaetter JG, Wang J, Yan J, Glimcher MJ (2006) Changes in bone microarchitecture and bone mineral density following experimental osteonecrosis of the hip in rabbits. Cells Tissues Organs 184:138–147. https://doi.org/10.1159/000099620
15. Deng B, Wang F, Yin L, Chen C, Guo L, Chen H, Gong X, Li Y, Yang L (2016) Quantitative study on morphology of calcified cartilage zone in OARSI 0 approximately 4 cartilage from osteoarthritic knees. Curr Res Transl Med 64:149–154. https://doi.org/10.1016/j.retram.2016.01.009
16. Bian W, Lian Q, Li D, Wang J, Zhang W, Jin Z, Qiu Y (2016) Morphological characteristics of cartilage-bone transitional structures in the human knee joint and CAD design of an osteochondral scaffold. Biomed Eng Online 15:82. https://doi.org/10.1186/s12938-016-0200-3
17. Aho OM, Finnila M, Thevenot J, Saarakkala S, Lehenkari P (2017) Subchondral bone histology and grading in osteoarthritis. PLoS ONE 12:e0173726. https://doi.org/10.1371/journal.pone.0173726
18. Eastell R, Szulc P (2017) Use of bone turnover markers in postmenopausal osteoporosis. Lancet Diab Endocrinol 5:908–923. https://doi.org/10.1016/S2213-8587(17)30184-5
19. Imhof H, Sulzbacher I, Grampp S, Czerny C, Youssefzadeh S, Kainberger F (2000) Subchondral bone and cartilage disease: a

rediscovered functional unit. Invest Radiol 35:581–588. https://doi.org/10.1097/00004424-200010000-00004
20. Kasiri S, Taylor D (2008) A critical distance study of stress concentrations in bone. J Biomech 41:603–609. https://doi.org/10.1016/j.jbiomech.2007.10.003
21. Taheri S, Yoshida T, Boker KO, Foerster RH, Jochim L, Flux AL, Grosskopf B, Lehmann W, Schilling AF (2021) Investigating the microchannel architectures inside the subchondral bone in relation to estimated hip reaction forces on the human femoral head. Calcif Tissue Int 109:510–524. https://doi.org/10.1007/s00223-021-00864-x
22. Zhang Q, Guo W, Chen Y, Zhao Q, Liu Z, Wang W (2021) The glycosaminoglycan content of hip cartilage in osteonecrosis of femoral head: evaluation with delayed gadolinium-enhanced magnetic resonance imaging of cartilage. Cartilage 12:70–75. https://doi.org/10.1177/1947603518803732
23. Raman S, FitzGerald U, Murphy JM (2018) Interplay of inflammatory mediators with epigenetics and cartilage modifications in osteoarthritis. Front Bioeng Biotechnol 6:22. https://doi.org/10.3389/fbioe.2018.00022
24. Ferrao Blanco MN, Bastiaansen-Jenniskens YM, Chambers MG, Pitsillides AA, Narcisi R, van Osch G (2021) Effect of inflammatory signaling on human articular chondrocyte hypertrophy: potential involvement of tissue repair macrophages. Cartilage 13:168S-174S. https://doi.org/10.1177/19476035211021907
25. Kennedy OD, Herman BC, Laudier DM, Majeska RJ, Sun HB, Schaffler MB (2012) Activation of resorption in fatigue-loaded bone involves both apoptosis and active pro-osteoclastogenic signaling by distinct osteocyte populations. Bone 50:1115–1122. https://doi.org/10.1016/j.bone.2012.01.025
26. Nielsen AW, Klose-Jensen R, Hartlev LB, Boel LWT, Thomsen JS, Keller KK, Hauge EM (2019) Age-related histological changes in calcified cartilage and subchondral bone in femoral heads from healthy humans. Bone 129:115037. https://doi.org/10.1016/j.bone.2019.115037